

Supporting Information

Interface Engineering of Amorphous/Crystalline Heterojunction with Synergistic Ru Doping for Efficient Hydrazine Oxidation Assisted Overall Water Splitting

Zhengyuan Liu^{a, b}, Yanyan Li^a, Haoran Guo^a, Jiayang Zhao^a, Haotian Zhang^c, Rui Song^{a*}

^aSchool of Chemical Sciences, University of Chinese Academy of Sciences (UCAS), 19 Yuquan Road, Shijingshan District, Beijing, 100049, P R China

^bSino-Danish College, University of Chinese Academy of Sciences (UCAS), P R China

^cBeijing National Laboratory for Molecular Sciences, College of Chemistry, Peking University, 5 Yiheyuan Road, Haidian District, Beijing, 100871, PR China

*Email: rsong@ucas.ac.cn

Content

1. Experimental Details	1
1.1. Sample preparation	1
1.1.1. Chemicals and Materials	1
1.1.2. Synthesis of Ni ₃ S ₂	1
1.1.3. Synthesis of Ru-Ni ₃ S ₂	1
1.1.4. Synthesis of the Pt/C and IrO ₂	1
1.2. Characterization	2
1.3. Electrochemical measurement	3
1.3.1. Calculation of electrochemical surface area (ECSA).....	3
1.3.2. Turnover frequency (TOF) calculations.....	4
1.4. DFT calculation	5
2. Results and Discussion	7
3. Reference	31

1. Experimental Details

1.1. Sample preparation

1.1.1. Chemicals and Materials

Sodium orthovanadate (Na_3VO_4 , 99%, dodecahydrate), thioacetamide ($\text{C}_2\text{H}_5\text{NS}$, $\geq 98\%$), urea ($\text{CH}_4\text{N}_2\text{O}$, $\geq 99.5\%$), and ammonium fluoride (NH_4F , 98%) were purchased from Aladdin Industrial Company (Shanghai, China). anhydrous ethanol, ruthenium(III) chloride trihydrate ($\text{RuCl}_3 \cdot 3\text{H}_2\text{O}$, 98%), and iridium oxide (IrO_2 , 99.9%) were purchased from Shanghai Macklin Biochemical Technology Co., Ltd. Platinum carbon (Pt/C, 20 wt%) was purchased from TKK (Tanaka). Seawater is taken from Bohai Bay and centrifuged to remove suspended impurities from the water. Other than that, all other reagents received were used without further purification. Deionized water ($18.2 \text{ M}\Omega \text{ cm}$) was used in all the experiments.

1.1.2. Synthesis of Ni_3S_2

The synthesis strategy of Ni_3S_2 was similar to that of $\text{VO}_x/\text{Ni}_3\text{S}_2$, Only no Na_3VO_4 for Ni_3S_2 , other conditions are the same.

1.1.3. Synthesis of Ru- Ni_3S_2

To get the same loading of Ru species, the as-synthesized Ni_3S_2 was directly transferred into a 25 mL beaker containing 20 mL solution with the same concentration as that in the synthesis of Ru- $\text{VO}_x/\text{Ni}_3\text{S}_2$ and kept for one hour reaction at 90°C .

1.1.4. Synthesis of the Pt/C and IrO_2

For comparison, 5 mg of Pt/C (20%Pt) or IrO_2 and 80 μL of 5 wt% Nafion solution were dispersed in 920 μL of isopropyl alcohol by sonication for 30 min. Then the 400 μL homogeneous suspension was drop-cast onto a Ni foam electrode where the total effective loading surface area of noble-metal catalysts was $0.5 \times 0.5 \times 2 \text{ cm}^2$, and the mass loading was 1.0 mg cm^{-2} .

1.2. Characterization

- 1) Scanning electron microscopy (SEM) was carried out on a Hitachi SU8220.
- 2) Transmission electron microscopy (TEM) and energy-dispersive X-ray spectroscopy (EDS) elemental mapping attached to the TEM was performed on an FEI Talos 200X instrument operating a FEG cathode at 200 kV and equipped with the Super-X in-column EDS detector.
- 3) X-ray diffraction (XRD) was characterized on a Bruker D8 diffractometer with Cu K α ($\lambda = 1.5406 \text{ \AA}$) radiation.
- 4) Raman spectra were examined using a Renishaw Invia Raman spectrometer with a 532 nm laser source.
- 5) X-ray photoelectron spectra (XPS) were measured by a Thermo escalab 250XI X-ray photoelectron spectrometer with an Al K α X-ray radiation (1486 eV).
- 6) The contact angle of gas (air) bubbles on the electrode materials under water was measured by the captive bubble method using a droplet shape analyzer DSA100, Germany.
- 7) The inductively coupled plasma optic emission spectrometer (ICP-OES) was carried out by Agilent ICP-OES 730.
- 8) Electron paramagnetic resonance (EPR) is measured by an A300-10/12 of Bruker, Germany.

1.3. Electrochemical measurement

A standard three-electrode setup on CHI 660E electrochemical workstation was used to conduct all the electrochemical measurements. The working electrodes were self-supported electrodes ($0.5 \times 0.5 \times 2 \text{ cm}^2$) while the counter electrode and the reference electrode were Pt sheet rod and Hg/HgO (filled in 1 M KOH), respectively. To measure the performance of HER and OER, multiple cyclic voltammetry (CV) scans were performed until the electrodes reached a stable state, followed by linear sweep voltammetry (LSV) with a scan rate of 5 mV s^{-1} in 1 M KOH solution. The HzOR performance was measured in alkaline freshwater (1 M KOH + 0.5 M N_2H_4) using the typical three-electrode configuration. Electrochemical impedance spectroscopy (EIS) measurements were carried out for HER, OER, and HzOR at the potential of -1.024 V, 0.6 V, and -1 V (vs. RHE) over a frequency range from 100 kHz to 0.01 Hz with an amplitude of 5 mV. The Faraday efficiency was tested using an H-type electrolytic cell assembled with a Nafion membrane (Nafion 211) and sealed with silicone sealant (Kraft K-704N). The polarization curves were corrected using 85% iR compensation and the potentials were referenced to the reversible hydrogen electrode (RHE), with all potentials mentioned in the manuscript referring to potentials vs. RHE ($E_{vs.RHE} = E_{vs.Hg/HgO} + 0.098 + 0.059 \times pH$).

A self-supported electrode of $0.5 \times 0.5 \times 2 \text{ cm}^2$ was used for stability test. To maintain the hydrazine concentration within a certain range during the long-term stability test, 1 mL 0.5M N_2H_4 was injected into the electrolytic cell with a syringe every 12 hours.

1.3.1. Calculation of electrochemical surface area (ECSA)

To estimate the effective electrode surface areas of various samples, the researchers conducted cyclic voltammetry (CV) in 1 M KOH. A series of CV measurements were performed at different scan rates (20, 40, 60, 80, 100, 120 mV/s) in the -0.8~-0.6 V vs. Hg/HgO, with the sweep segments set to 10 for consistency. By plotting $\Delta J = (J_{anodic} - J_{cathodic})/2$ versus the scan rate v_s , and following with a linear fit, the double layer capacitance (C_{dl}) can be estimated according to the slope, which can be expressed using the equation¹:

$$C_{dl} = \frac{d\Delta J}{dv_s} \quad \backslash * \text{MERGEFORMAT (1.1)}$$

The electrochemically active surface area (ECSA) of a material was calculated by taking the ratio of its top C_s , which gives an indication of its electrochemical activity.

$$ECSA = \frac{C_{dl}}{C_s} \quad \backslash * MERGEFORMAT (1.2)$$

where C_s is the specific capacitance, chosen as $C_s = 0.040 \text{ mF cm}^{-2}$ in 1 M KOH.

1.3.2. Turnover frequency (TOF) calculations

The turnover frequency (TOF) was estimated by the following equation²:

$$TOF = \frac{I}{\alpha n F} \quad \backslash * MERGEFORMAT (1.3)$$

where I is current (A) during the linear sweep voltammetry (LSV) tests in 1 M KOH, n is the number of active sites (mol), F is the Faraday constant (96485 C mol^{-1}), α as the factor with a value of 2 is introduced to consider the consumed electrons generating one H_2 from water.

The number of active sites (mol) was calculated by the following equation:

$$n = \frac{Q}{2F} = \frac{It}{2F} = \frac{IV}{2Fv} \quad \backslash * MERGEFORMAT (1.4)$$

where Q is the voltammetric charge, F is the Faraday constant (C mol^{-1}), I stands for the current (A), t is the time (s), V is the voltage (V) and v is the scanning rate (V s^{-1}).

1.3.3. In-situ Raman spectrum

The in-situ Raman test was conducted by combining the CHI 660E electrochemical workstation and the Renishaw Invia Raman spectrometer. For in-situ Raman testing of OER, a chronoamperometric method is employed on the electrochemical workstation, with potential settings ranging from 1.1V to 2.0V in increments of 0.1V, each maintained for a duration of 120 seconds. Subsequently, the electrode is removed and transferred to the Raman spectrometer to record the Raman spectra. For in-situ Raman testing of the HzOR, a similar procedure is followed, with potential settings ranging from -0.1 V to 0.3 V in increments of 0.05 V.

1.4. DFT calculation

First-principles calculations were performed within the density functional theory framework³. The projector-augmented wave (PAW) method^{4,5} and the generalized gradient approximation (GGA)⁶ for the exchange-correlation energy functional, as implemented in the Vienna ab initio simulation package (VASP)⁷⁻¹⁰ were used. The GGA calculation was performed with the Perdew-Burke-Ernzerhof (PBE)¹¹ exchange-correlation potential. Considered long-range interaction between molecules/intermediates and surface, Van der Waals interactions were considered using DFT-D3 correlation¹². A combined supercell slab model was built to simulate the surface of Ni₃S₂ and heterostructure models. To avoid effects come from other slabs, a vacuum of 15 Å was added along z direction. The convergence criterion of geometry relaxation was set to 0.03 eV·Å⁻¹ in force on each atom. The energy cutoff for plane wave-basis was set to 600 eV. The K points were sampled with 3×3×1 by Monkhorst-Pack method.

The change in free energy (ΔG) of per reaction step was calculated as following¹³:

$$\Delta G = \Delta E + \Delta ZPE - T \cdot \Delta S + \Delta G_U + \Delta G_{pH}$$

Where ΔE is the change of the total reaction energy obtained from DFT calculation, ΔZPE is the change of the zero-point energy, T is the temperature (300K), and ΔS is the change of the entropy. $\Delta G_U = -eU$, where U is the potential at the electrode and e is the transferred charge. $\Delta G_{pH} = k_B \cdot T \times \ln 10 \times pH$, where k_B is the Boltzmann constant and $T = 300$ K. In this work, the influence of pH was neglected.

For HER, the hydrogen adsorption free energy (ΔG_{H^*}) was calculated by the following equation¹⁴:

$$\Delta G_{H^*} = E_{H^*} + 0.24 \text{ eV}$$

Where ΔE_{H^*} is defined by the following equation:

$$\Delta E_{H^*} = E_{H^*} - (E_* + 1/2 E_{H_2})$$

Where E_{H^*} is the total energy of H atom on the support, E_* is the total energy of support, E_{H_2} is the energy of the gas H_2 calculated by setting the isolated H_2 in a box of $10.0 \text{ \AA} \times 10.0 \text{ \AA} \times 10.0 \text{ \AA}$. The Gibbs free energy for the well-known highly efficient Pt catalyst is near-zero as $|\Delta G_{ads}| \approx 0.09 eV^{15}$.

2. Results and Discussion

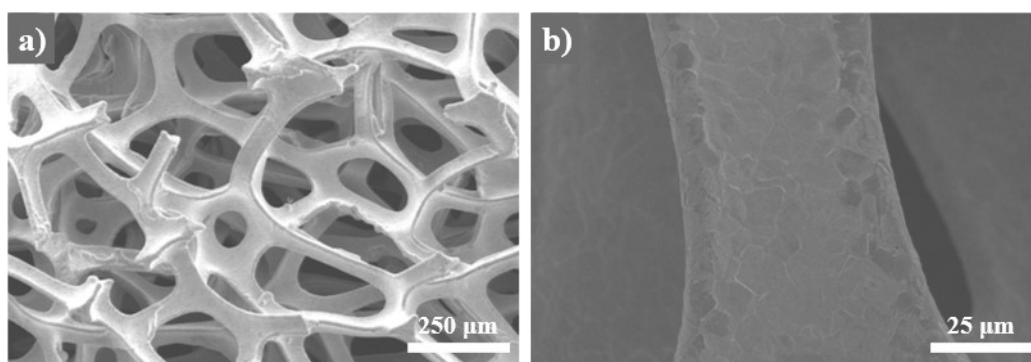


Fig. S1 (a) Low-magnification and (b) high-magnification SEM images of pre-treated bare Ni foam.

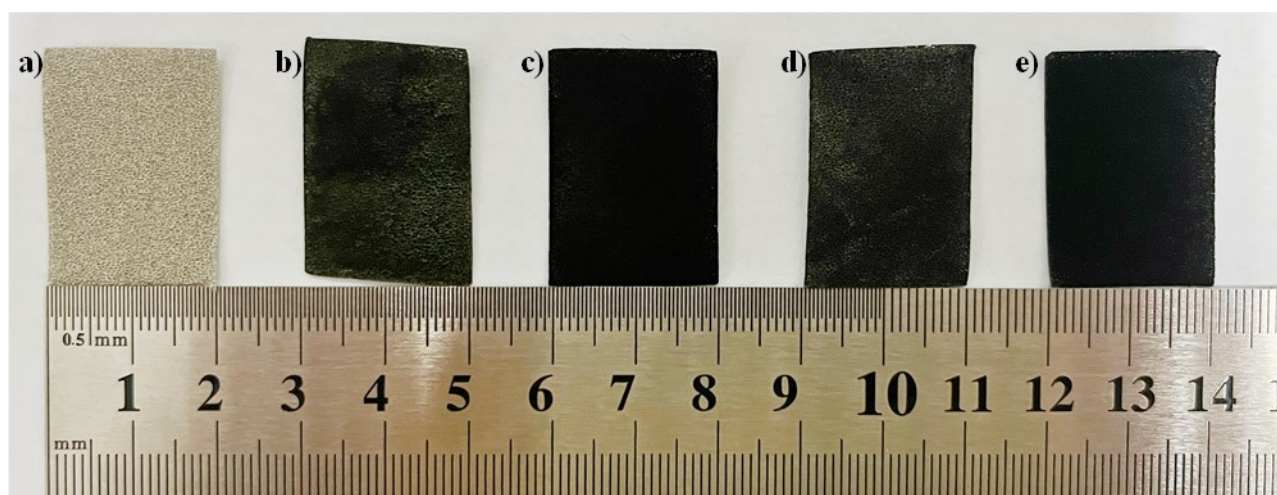


Fig. S2 Photographs of (a) bare NF, (b) Ni_3S_2 , (c) $\text{V-Ni}_3\text{S}_2$, (d) $\text{Ru-Ni}_3\text{S}_2$, and (e) $\text{Ru/V-Ni}_3\text{S}_2$.

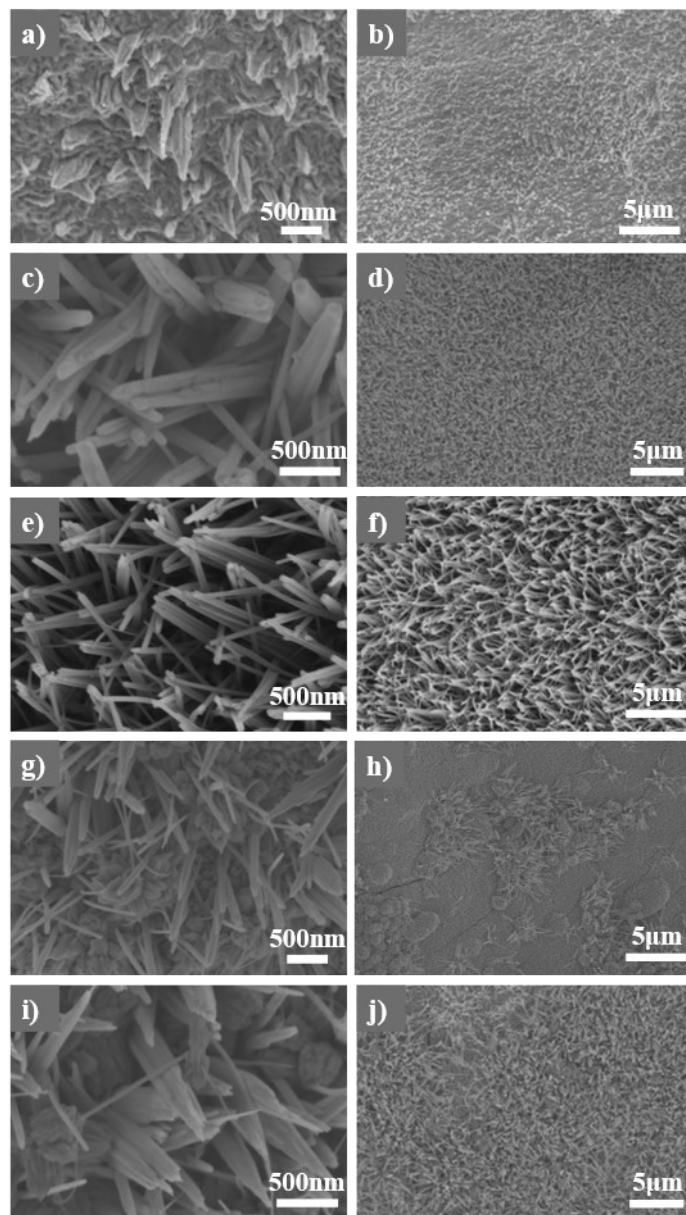


Fig. S3 SEM images at low and high magnification with different Na_3VO_4 doses of **(a, b)** 0 mmol, **(c, d)** 0.05 mmol, **(e, f)** 0.1 mmol, **(g, h)** 0.2 mmol and **(i, j)** 0.3 mmol.

When no vanadium (V) source is added, the NF surface has an inhomogeneous granular micro-nanostructure. When 0.05 mmol sodium orthovanadate (Na_3VO_4) is added, uniform nanorods grow on the NF surface, but the SEM images with high magnification show some fragmentation on the surface of the nanorods. When the V amount increases to 0.1 mmol, the surface fragmentation of nanorods is improved and the overall appearance of finer arrays of smooth nanorods is observed. With further increase of Na_3VO_4 dosage, the uniform nanorod arrays are destroyed and cracks appear in some areas under low magnification.

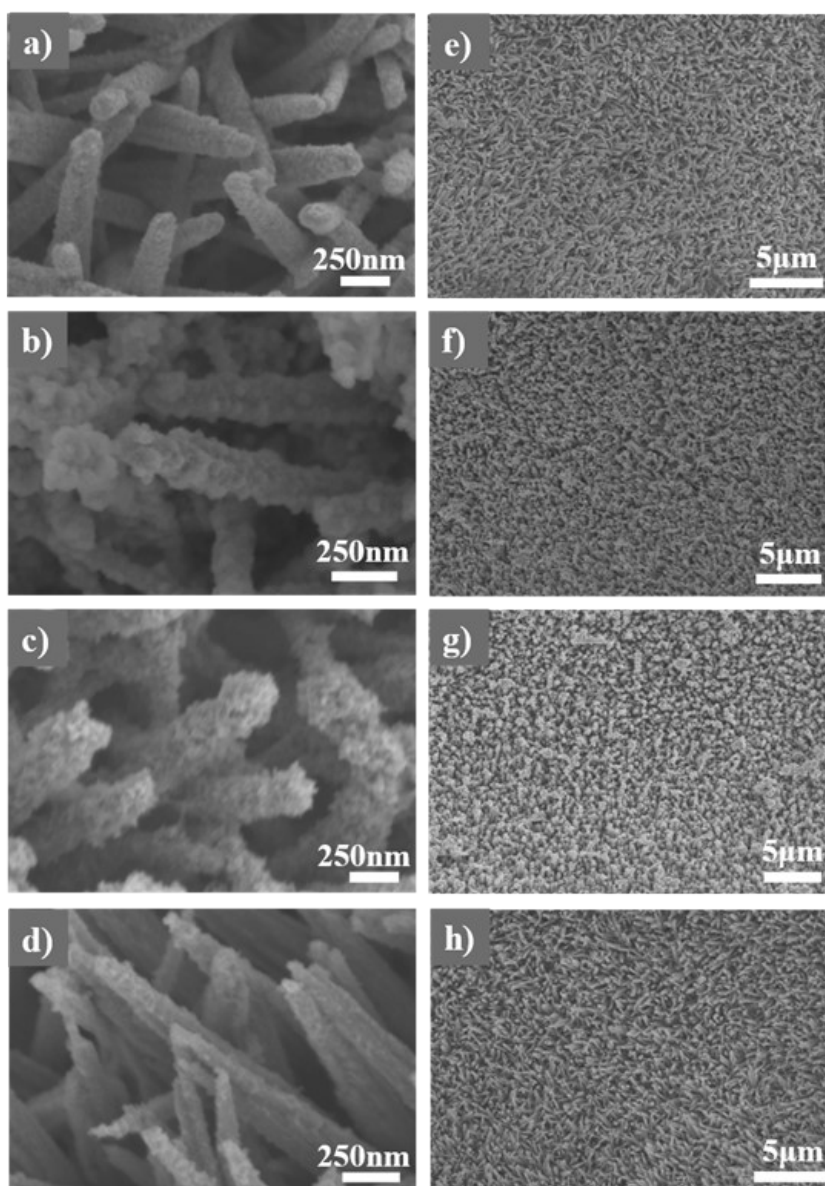


Fig. S4 SEM images of VO_x/Ni₃S₂ immersed in RuCl₃ solution for (a) 0.5 h, (b) 1 h, (c) 2 h, and (d) 3 h. (e-h) SEM images of the corresponding Ru-VO_x/Ni₃S₂.

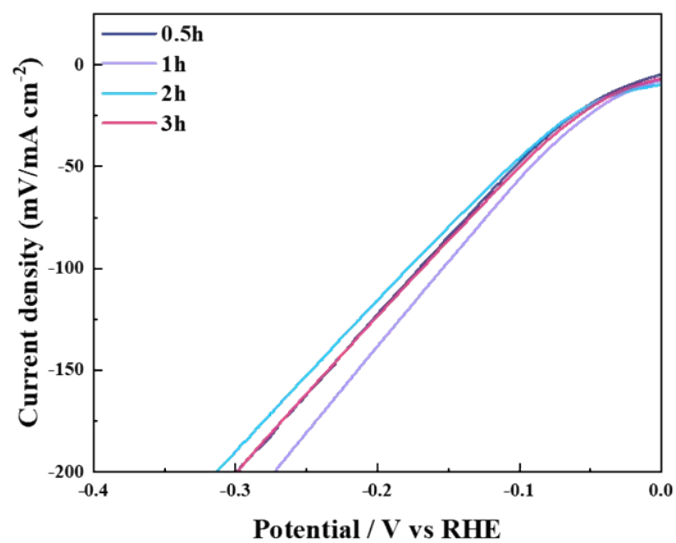


Fig. S5 LSV curves of Ru-VO_x/Ni₃S₂ with different impregnation time.

For different impregnation times, the morphological differences are not significant. However, it can be seen from the LSV curves that the performance of 1 h immersion in RuCl₃ solution is slightly better than that of the samples with other immersion time.

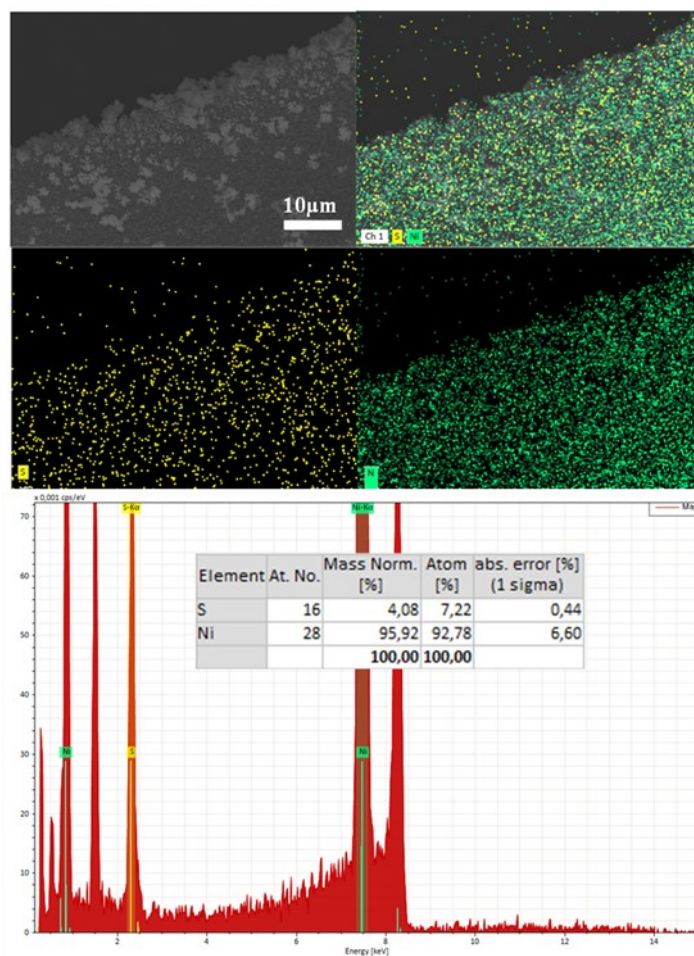


Fig. S6 SEM-EDS elemental mapping images of Ni_3S_2 .

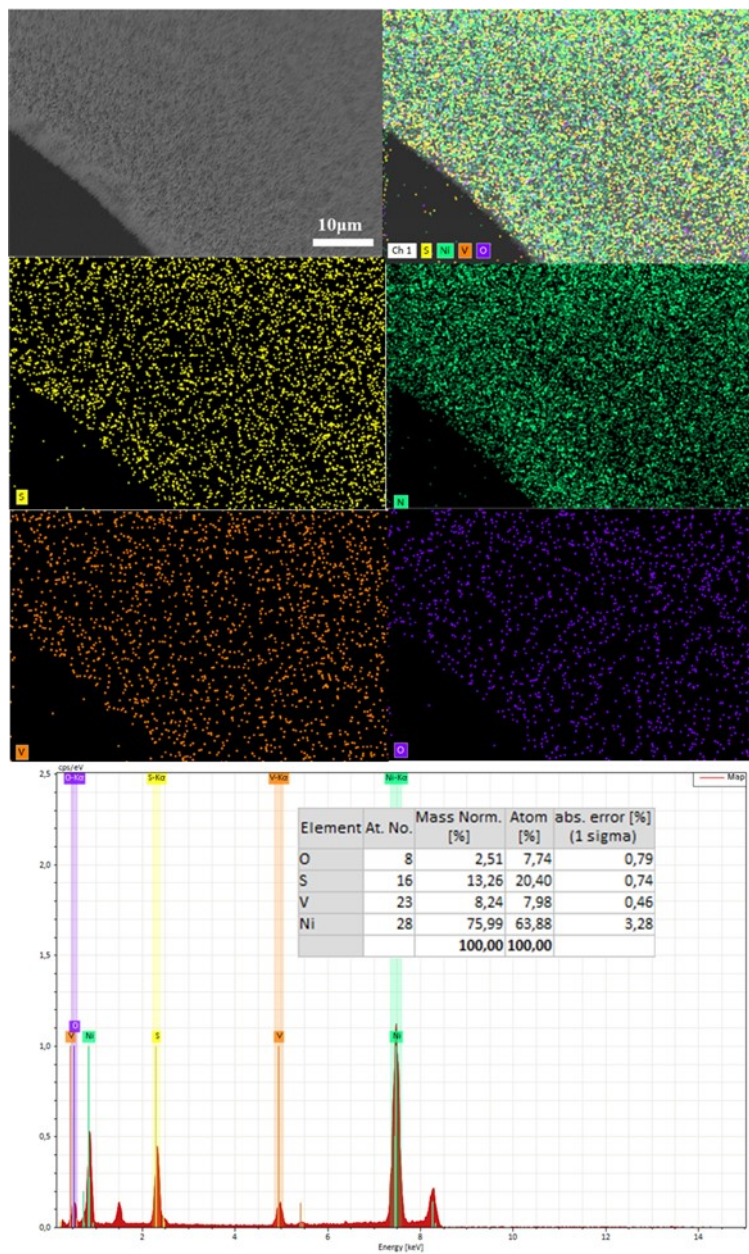


Fig. S7 SEM-EDS elemental mapping images of $\text{VO}_x/\text{Ni}_3\text{S}_2$.

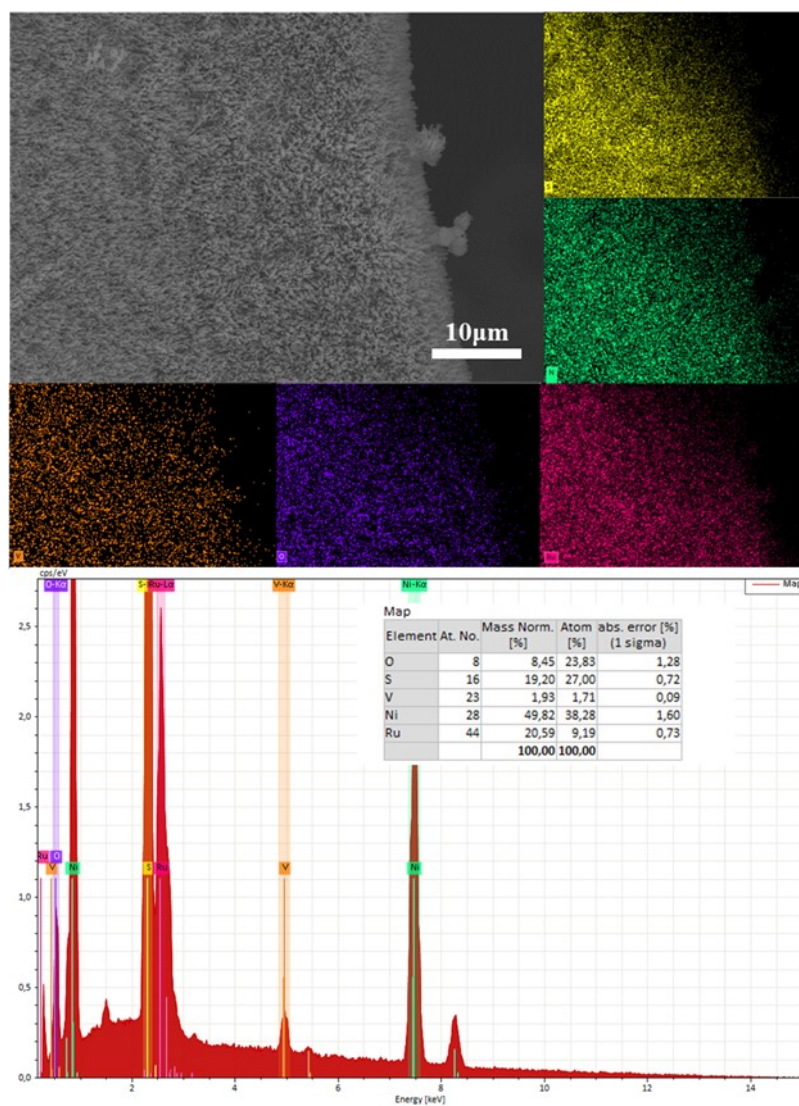


Fig. S8 SEM-EDS elemental mapping images of Ru-VO_x/Ni₃S₂.

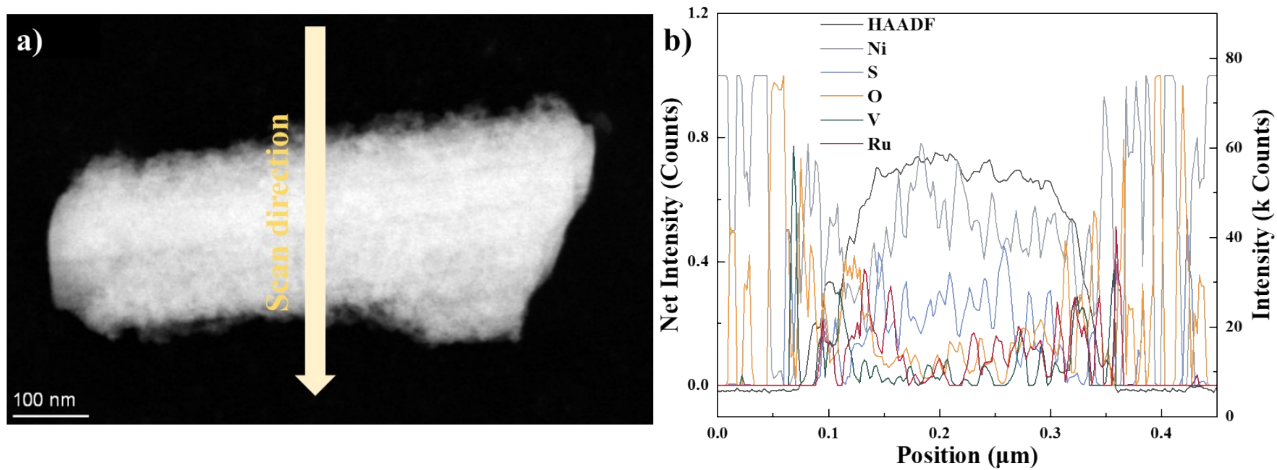


Fig. S9 TEM energy-dispersive X-ray spectroscopy (EDS) linear scan.

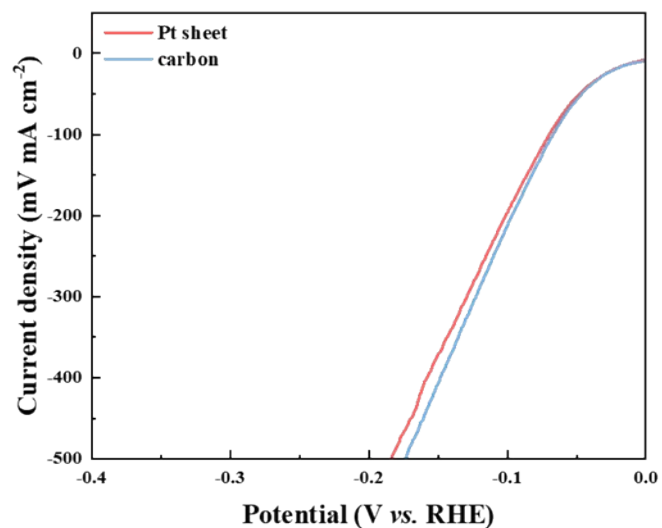


Fig. S10 The LSV curves of Ru-VO_x/Ni₃S₂ with Pt sheet and carbon rod as the counter electrode.

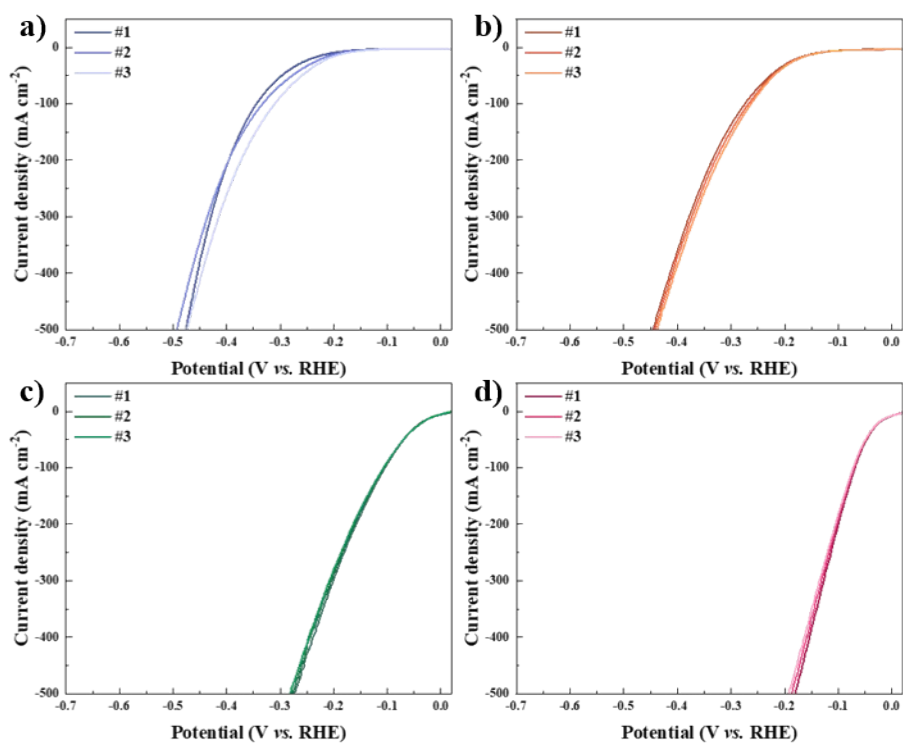


Fig. S11 The LSV curves of HER performance measurement for three times (a) Ni₃S₂ (b) VO_x/Ni₃S₂ (c) Ru-Ni₃S₂ and (d) Ru-VO_x/Ni₃S₂.

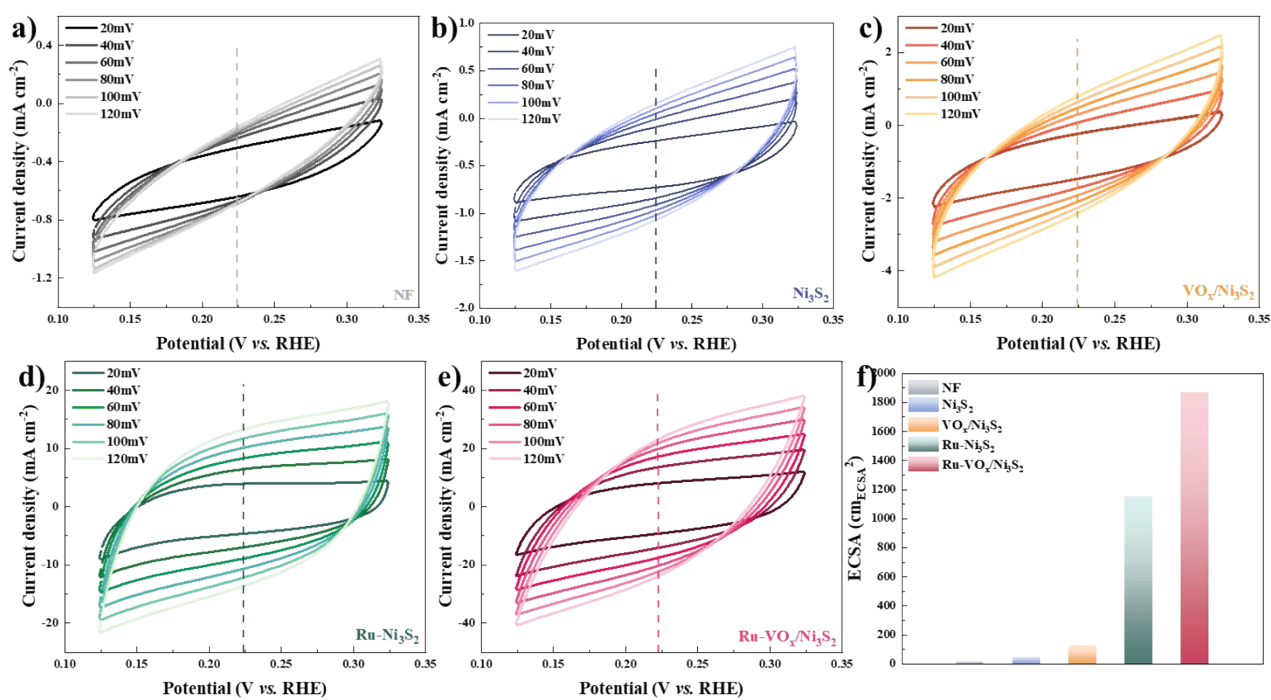


Fig. S12 The CV curves of (a) NF, (b) Ni₃S₂, (c) VO_x/Ni₃S₂, (d) Ru-(Ni/Fe)C₂O₄, (e) Ru-VO_x/Ni₃S₂ at varying scan rates (20, 40, 60, 80, 100, 120 mV s⁻¹) and (f) ECSA values of all catalysts.

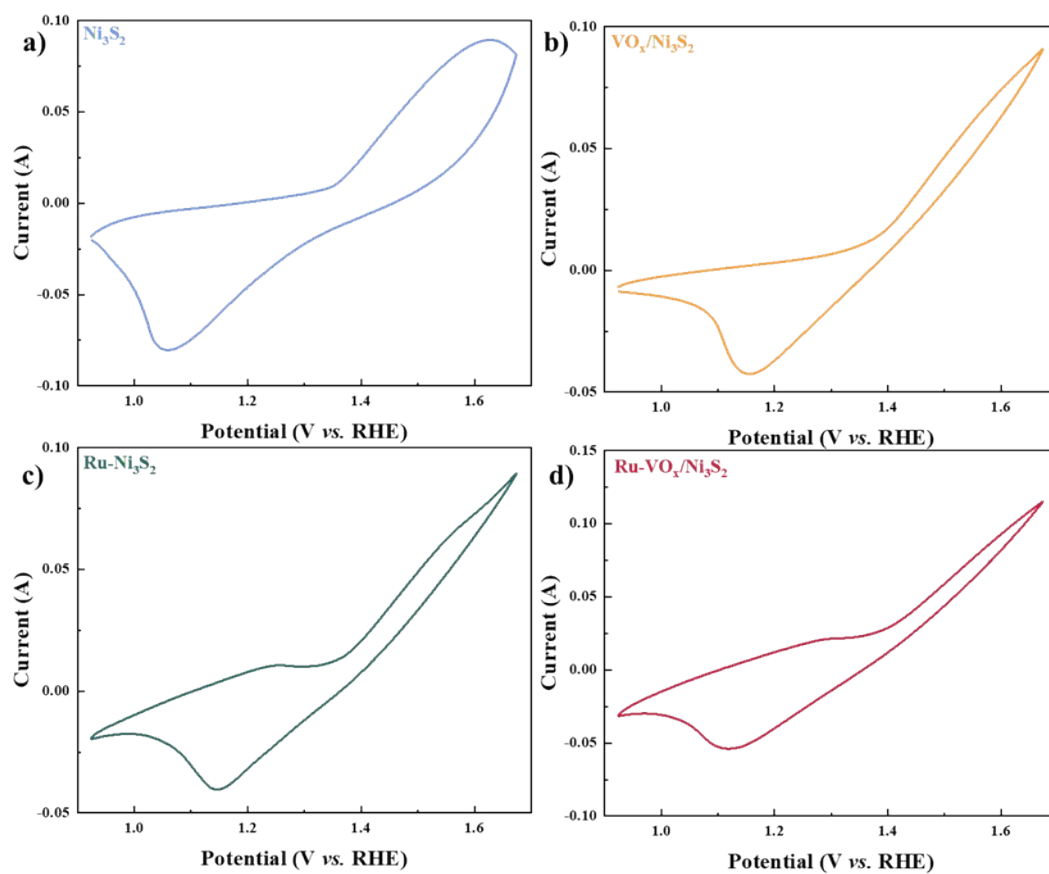


Fig. S13 The CV curves of as-prepared (a) Ni_3S_2 (b) $\text{VO}_x/\text{Ni}_3\text{S}_2$ (c) $\text{Ru-Ni}_3\text{S}_2$ and (d) $\text{Ru-VO}_x/\text{Ni}_3\text{S}_2$ in 1 M KOH at 100 mV.

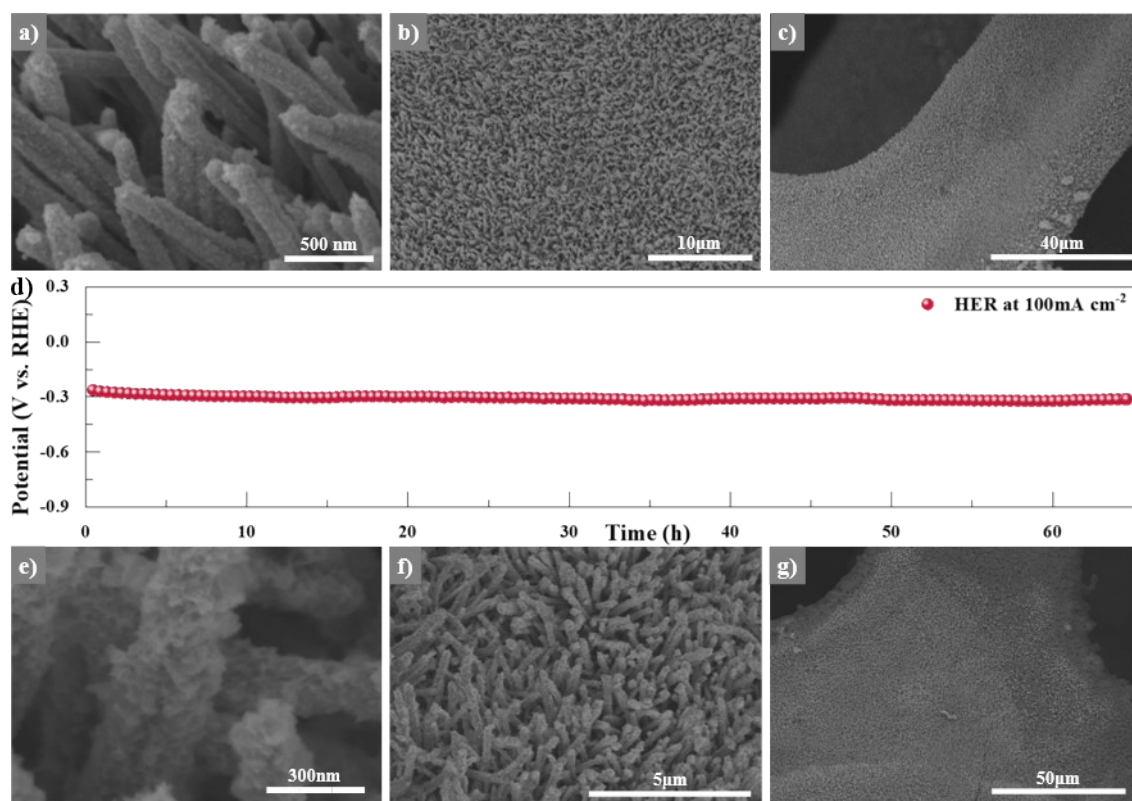


Fig. S14 (a-c) SEM image of Ru-VO_x/Ni₃S₂ after 100 h HER stability test at 10 mA cm⁻². (d) Chronopotentiometry curve of Ru-VO_x/Ni₃S₂ at the constant current density of 100 mA cm⁻² (without *i*R compensation). (e-g) SEM image of Ru-VO_x/Ni₃S₂ after 65 h HER stability test at 100 mA cm⁻².

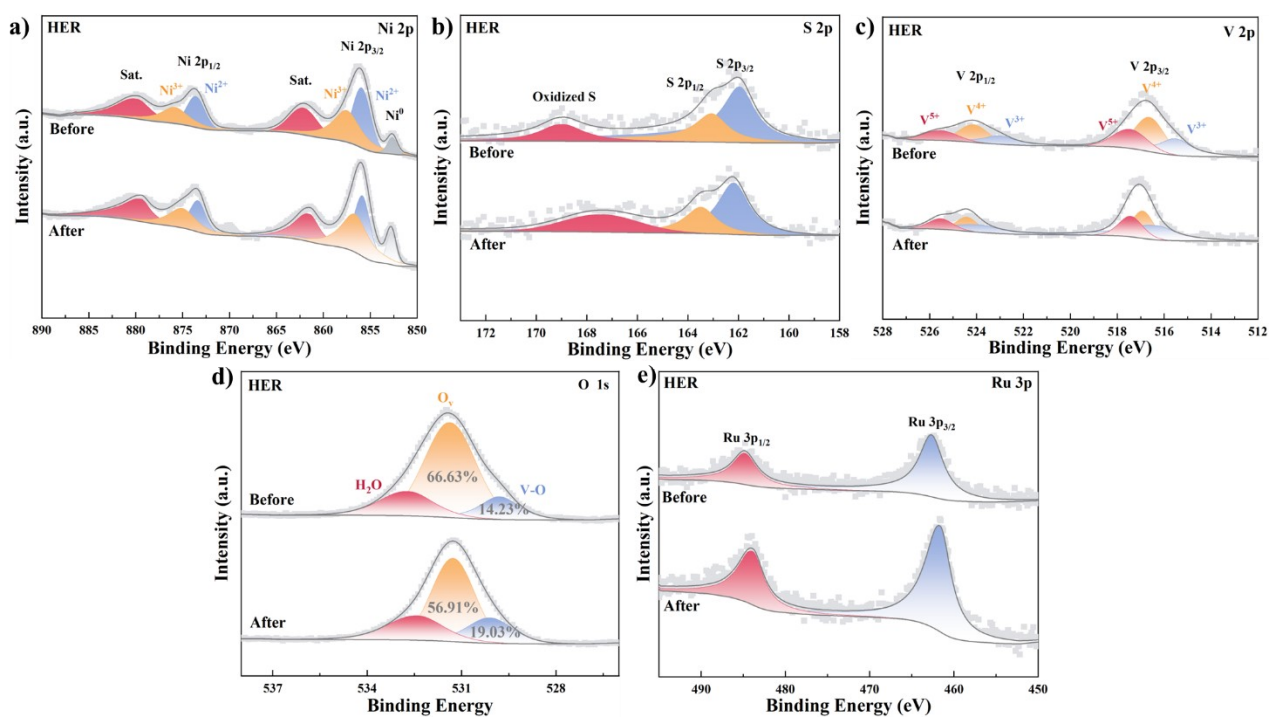


Fig. S15 The XPS spectra of (a) Ni 2p, (b) S 2p, (c) V 2p, (d) O 1s, and (e) Ru 3p for the Ru-VO_x/Ni₃S₂ electrocatalyst after the HER stability test conducted at 10 mA cm⁻².

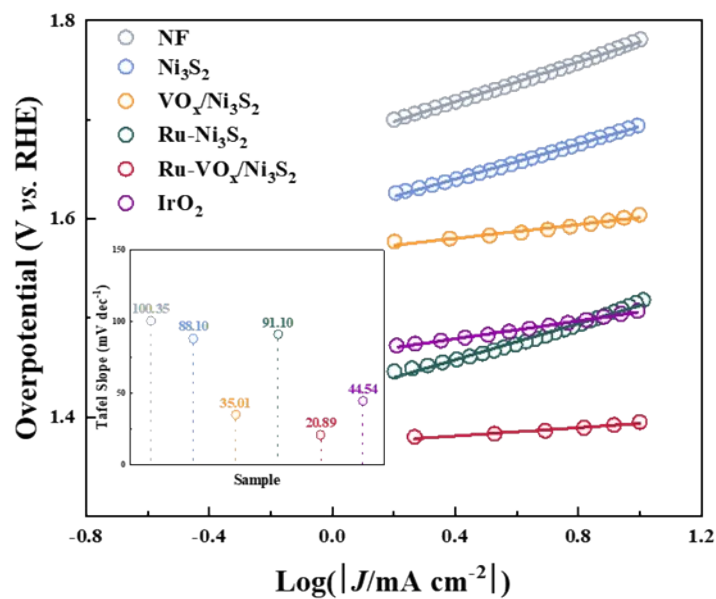


Fig. S16 Tafel plots of NF, Ni₃S₂, VO_x/Ni₃S₂, Ru-Ni₃S₂, Ru-VO_x/Ni₃S₂, and IrO₂ electrodes for the OER process.

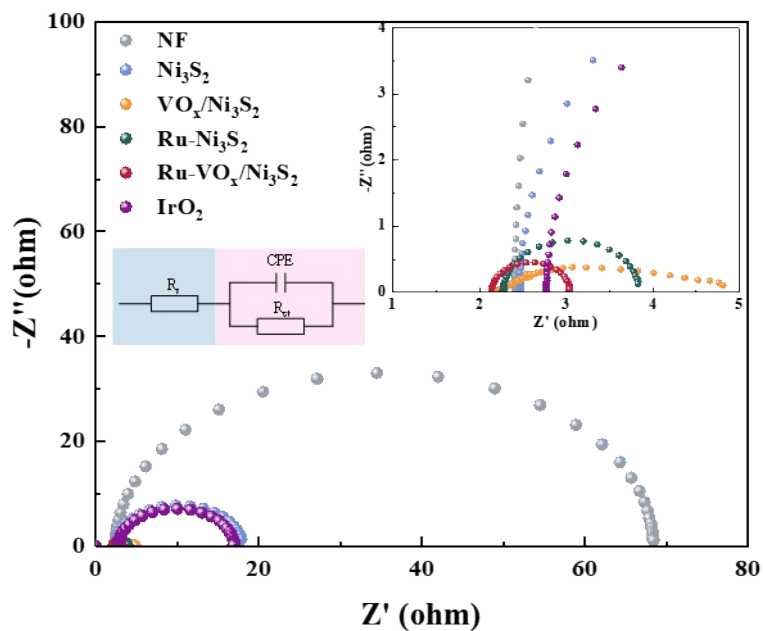


Fig. S17 Nyquist plots of NF, Ni₃S₂, VO_x/Ni₃S₂, Ru-Ni₃S₂, Ru-VO_x/Ni₃S₂ and IrO₂ electrodes in 1 M KOH at the potential of 1.524V.

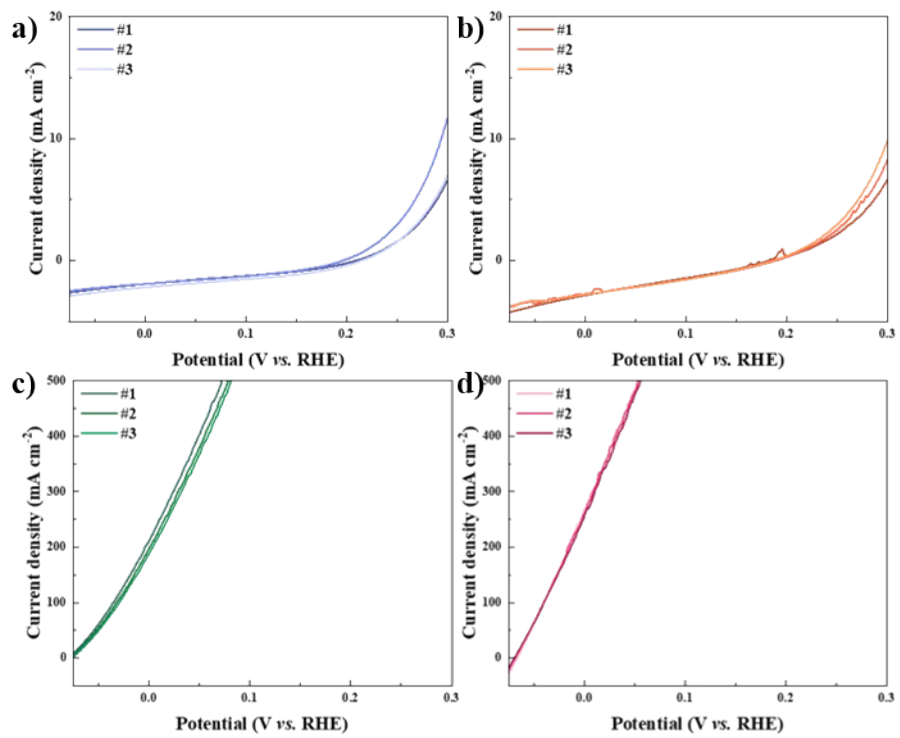


Fig. S18 The LSV curves of HzOR performance measurement for three times. **(a)** Ni_3S_2 **(b)** $\text{VO}_x/\text{Ni}_3\text{S}_2$ **(c)** $\text{Ru-Ni}_3\text{S}_2$ and **(d)** $\text{Ru-VO}_x/\text{Ni}_3\text{S}_2$.

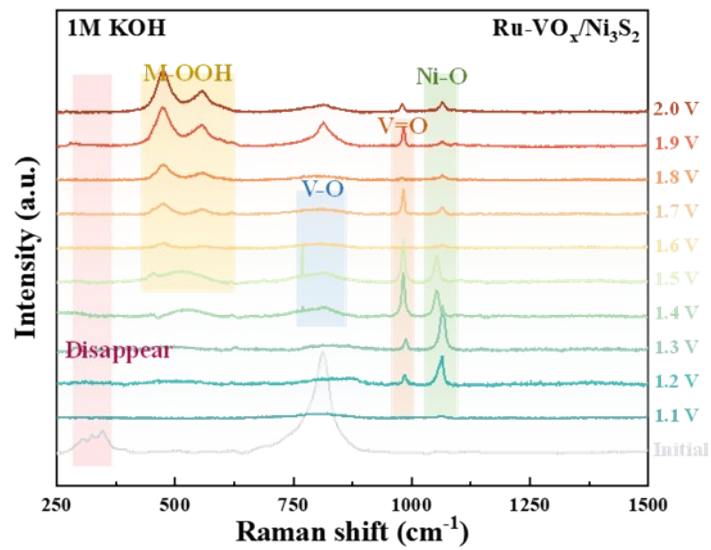


Fig. S19 In-situ Raman spectra of Ru-VO_x/Ni₃S₂ during OER process in 1.0 M KOH.

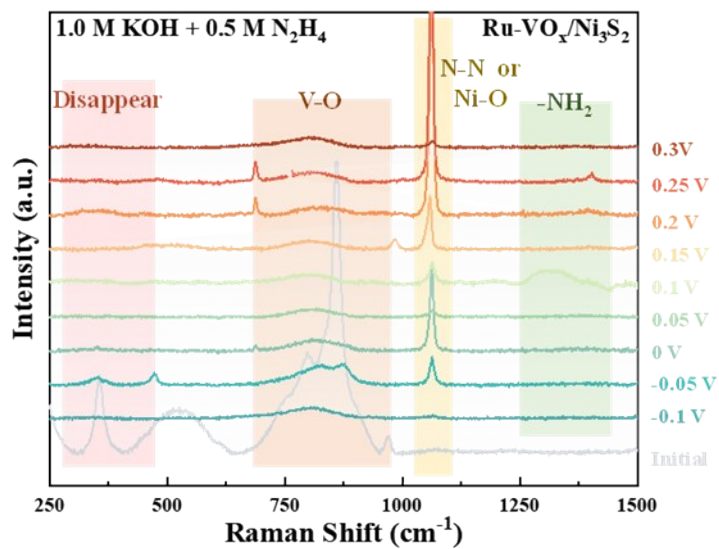


Fig. S20 In-situ Raman spectra of Ru-VO_x/Ni₃S₂ during HzOR process in 1.0 M KOH + 0.5 M N₂H₄.

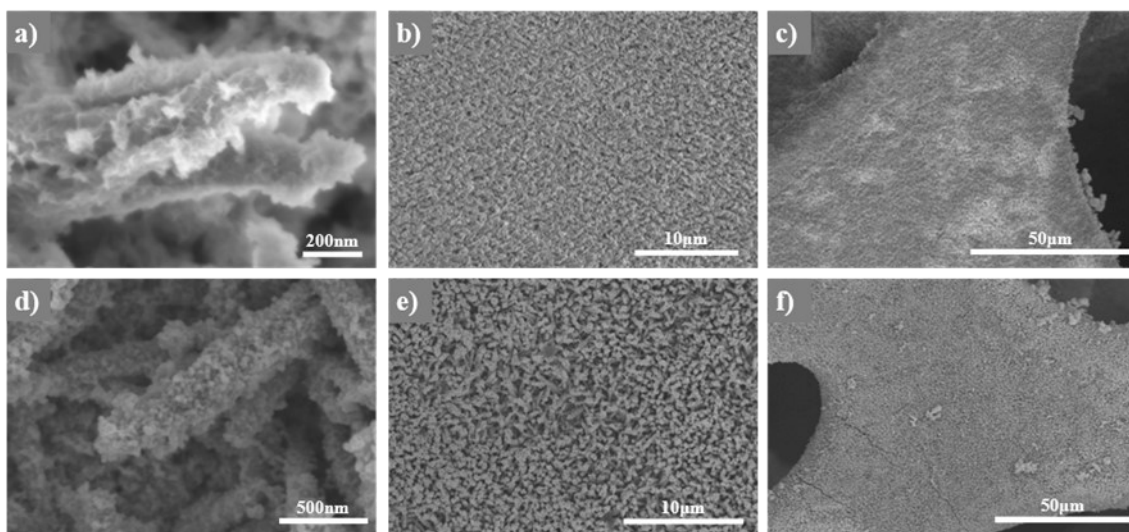


Fig. S21 SEM images after stability test for (a-c) OER and (d-f) HzOR process.

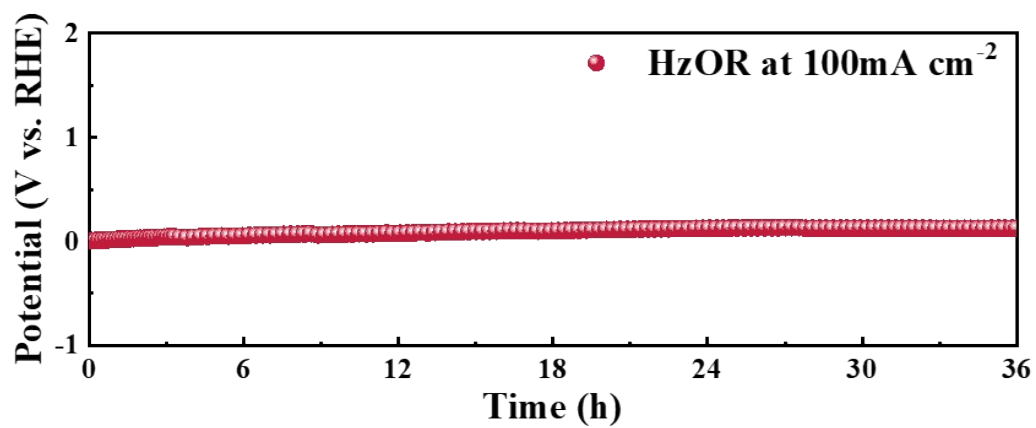


Fig. S22 Chronopotentiometry curve of Ru-VO_x/Ni₃S₂ at the constant current density of 100 mA cm⁻² (without *i*R compensation).

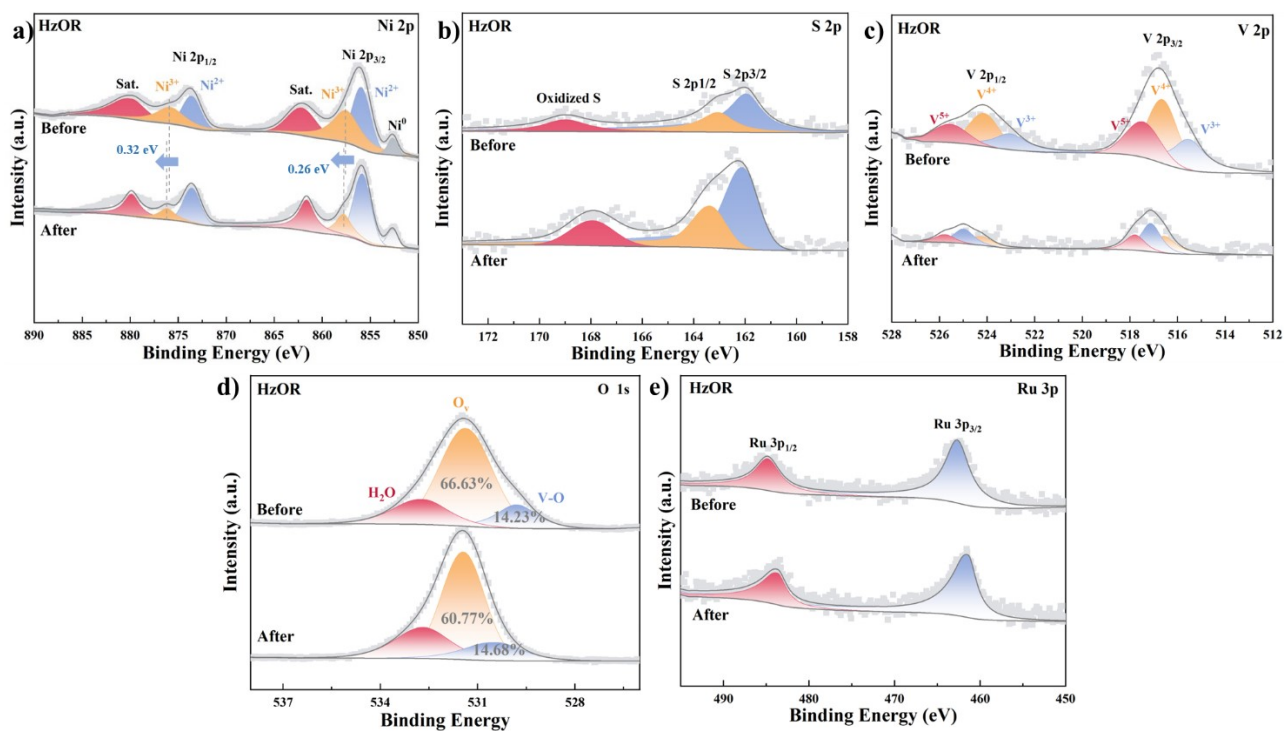


Fig. S23 The XPS spectra of (a) Ni 2p, (b) S 2p, (c) V 2p, (d) O 1s, and (e) Ru 3p for the Ru-VO_x/Ni₃S₂ electrocatalyst after the HzOR stability test conducted at 10 mA cm⁻².



Fig. S24 Device diagram for measuring Faraday efficiency at the ambient condition. The electrolyte in the electrolytic cell is separated by a Nafion membrane.

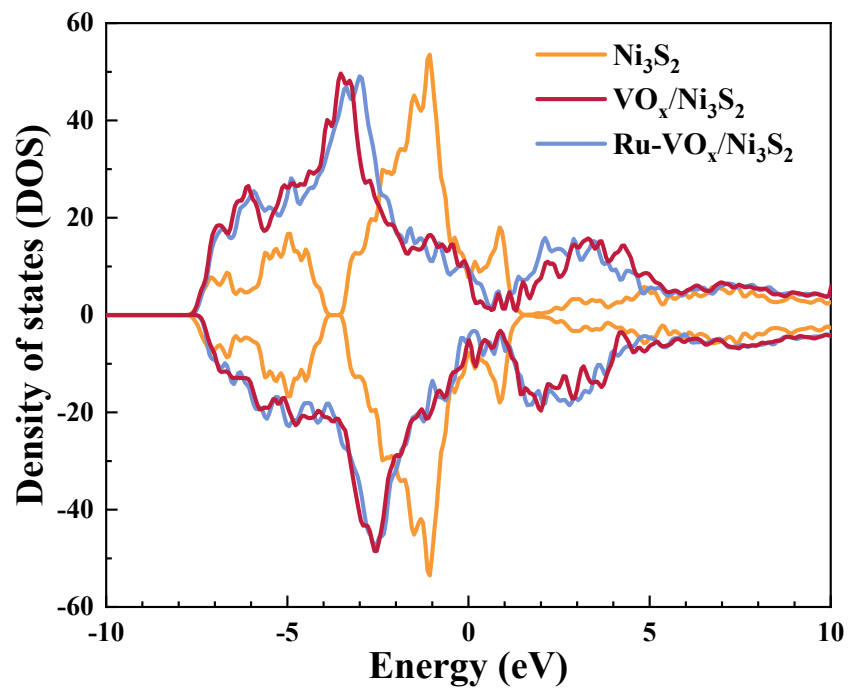


Fig. S25 The density of states of Ni_3S_2 , $\text{VO}_x/\text{Ni}_3\text{S}_2$, and $\text{Ru-VO}_x/\text{Ni}_3\text{S}_2$ models.

Table S1 HER performance of the as-prepared catalysts

HER Performance	NF	Ni ₃ S ₂	VO _x /Ni ₃ S ₂	Ru-Ni ₃ S ₂	Ru-VO _x /Ni ₃ S ₂	Pt/C
η_{10} (mV)	220	229	190	16	7	31
η_{500} (mV)	527	474	498	280	195	397
Tafel slope (mV dec ⁻¹)	176.38	190.18	230.57	39.55	35.05	65.52
j_0 (mA cm ⁻²)	1.00	0.67	1.03	4.91	11.26	2.68

* η represents overpotential: $\eta_{(HER)} = E_{(RHE)} - 0V$

Table S2 Performance comparison of overpotential, Tafel slope, and stability with recently reported Ru or Ni-based electrocatalysts in 1 M KOH

Materials	Overpotential η_{10} (mV)	Tafel slope (mV dec ⁻¹)	Stability		Ref.
			Current Density (mA cm ⁻²)	Time (h)	
Ru-VO_x/Ni₃S₂	7	31.32	100	65	This work
Ru/c-Ti ₃ C ₂ T _x /NF	37	60	100	14	16
Ru SAs-MoO _{3-x} /NF	36	41.3	50	50	2
RuCo-CAT/CC	46	32.1	10	15	17
Ru-NiFe-P	44	80	10	24	18
Ru/HMCs	26.93	41.26	100	12	19
Ru-CoV-LDH/NF	32	36.4	20	45	20
LN-Ru	33	45	-	-	21
Ru/NF	10	34	-	-	22
Ru-(Ni/Fe)C ₂ O ₄	42	39	100	65	1
Ru-NiFe-MOF/NFF	17	34.9	10	30	23
CPF-Fe/Ni	42	94.1	10	200	24
Ni ₅ P _{4-x} I _x /Ni ₂ P	45	41	-	-	25
NiSe ₂ NTA	88	78	10	12	26
Ni(OH) ₂ /MoS ₂ NF	95	62.1	10	50	27
Ni(OH) ₂ /NiSe ₂ /CC	82	60	10	12	28
NiFeCoS _x @FeNi ₃	88	116	10	40	29
Ni-LCO/C	114	72.7	10	25	30
MoS ₂ /Ni ₃ S ₂ /NF	93	85	15	10	31
Ni-GF/VC	128	80	10	20	32

Table S3 The R_s and R_{ct} values of the comparison materials for HER

EIS	NF	Ni ₃ S ₂	VO _x /Ni ₃ S ₂	Ru-Ni ₃ S ₂	Ru-VO_x/Ni₃S₂	Pt/C
R_{ct} (Ω)	133.8	172.7	58.8	1.6	0.6	4.1
R_s (Ω)	2.6	2.6	2.7	2.7	2.7	2.9

Table S4 HzOR performance of the as-prepared catalysts

HzOR Performance	VO _x /Ni ₃ S ₂	Ru-VO _x /Ni ₃ S ₂	IrO ₂
E ₁₀ (V)	0.308	-0.066	0.029
E ₁₀₀ (V)	-	-0.039	0.172
E ₅₀₀ (V)	-	0.082	-
Tafel slope (mV dec ⁻¹)	17.03	9.61	93.35

*E represents the potential vs. RHE.

Table S5 The R_s and R_{ct} values of the comparison materials for HzOR

EIS	NF	Ni ₃ S ₂	VO _x /Ni ₃ S ₂	Ru-Ni ₃ S ₂	Ru-VO _x /Ni ₃ S ₂	IrO ₂
R _{ct} (Ω)	186.7	208	69.48	1.28	0.55	11.08
R _s (Ω)	2.3	2.4	2.4	2.3	2.2	2.5

Table S6 HzOR performance comparison of overpotential, Tafel slope, and stability with recently developed Ru or Ni-based electrocatalysts in 1.0 M KOH + 0.5 M N₂H₄

Samples	Electrolyte	Potential	Stability		Ref.
	[KOH], [N ₂ H ₄]	<i>x</i> V @ <i>y</i> mA cm ⁻²	mA cm ⁻²	t (h)	
Ru-VO_x/Ni₃S₂	1.0M, 0.5 M	-0.066 V @ 100 mA cm⁻²	10		This work
Ru-FeP ₄ /IF	1.0M, 0.5M	0.027 V @ 100 mA cm ⁻²	100	20	33
Ru-Cu ₂ O/CF	-	-0.041 V @ 10 mA cm ⁻²	10	14	34
Au ₁ Pt ₈	1.0M, 0.5M	0.502 V @ 10 mA cm ⁻²	-	-	35
Cu ₁ Pd ₃ /C	1.0M, 0.5M	0.560 V @ 10 mA cm ⁻²	10	5	36
Pd NCs/NiFe	1.0M, 0.2M	0.050 V @ 10 mA cm ⁻²	-	-	37
PtCu-NA	1.0M, 1.0M	0.220 V @ 10 mA cm ⁻²	10	70	38
Ru/MPNC	1.0M, 0.5M	-0.039 V @ 10 mA cm ⁻²	10	10	39
<i>l</i> -Rh	1.0M, 0.1M	-0.002 V @ 10 mA cm ⁻²	10	20	40
Rh-NS-HCS	1.0M, 0.5M	0.084 V @ 10 mA cm ⁻²	10	10	41
RhIr MNs	1.0M, 0.5M	-0.012 V @ 10 mA cm ⁻²	10	12	42
CoP/Co-20	1.0M, 0.5M	-0.069 V @ 10 mA cm ⁻²	100	24	43
(Ni ₂ Co) _{0.85} Se/rGO	1.0M, 0.1M	0.124 V @ 10 mA cm ⁻²	50	24	44
Mn-CoS ₂	1.0M, 0.5M	0.077 V @ 10 mA cm ⁻²	10	40	45
N-Ni ₅ P ₄ @CoP/CFP	1.0M, 0.1M	-0.032 V @ 10 mA cm ⁻²	10	3	46
V _{41.7wt%} -Co-MOF	1.0M, 0.5M	-0.049 V @ 10 mA cm ⁻²	20	36	47
Cu-CoFe/Co/NC	1.0M, 0.5M	0.281 V @ 10 mA cm ⁻²	100	20	48
FeNiP-NPHC	1.0M, 0.5M	0.007 V @ 100 mA cm ⁻²	100	100	49
MoO ₂ /Co	1.0M, 0.5M	-0.073 V @ 10 mA cm ⁻²	20	28	50
(Co _{0.6} Ni _{0.4}) ₂ P@PC	1.0M, 0.5M	0 V @ 50 mA cm ⁻²	10	10	51

3. Reference

- 1 J. Zhao, H. Guo, Q. Zhang, Y. Li, L. Gu and R. Song, *Applied Catalysis B: Environmental*, 2023, **325**, 122354.
- 2 D. Feng, P. Wang, R. Qin, W. Shi, L. Gong, J. Zhu, Q. Ma, L. Chen, J. Yu, S. Liu and S. Mu, *Advanced Science*, **n/a**, 2300342.
- 3 W. Kohn and L. J. Sham, *Phys. Rev.*, 1965, **140**, A1133–A1138.
- 4 P. E. Blöchl, *Phys. Rev. B*, 1994, **50**, 17953–17979.
- 5 G. Kresse and D. Joubert, *Phys. Rev. B*, 1999, **59**, 1758–1775.
- 6 J. P. Perdew and Y. Wang, *Physical Review B*, 1992, **45**, 13244–13249.
- 7 G. Kresse and J. Hafner, *Phys. Rev. B*, 1993, **47**, 558–561.
- 8 G. Kresse and J. Furthmüller, *Phys. Rev. B*, 1996, **54**, 11169–11186.
- 9 L. Chen, L. Zhou, H. Lu, Y. Zhou, J. Huang, J. Wang, Y. Wang, X. Yuan and Y. Yao, *Chem. Commun.*, 2020, **56**, 9138–9141.
- 10 G. Kresse and J. Furthmüller, *Computational Materials Science*, 1996, **6**, 15–50.
- 11 J. P. Perdew, K. Burke and M. Ernzerhof, *Phys. Rev. Lett.*, 1996, **77**, 3865–3868.
- 12 S. Grimme, J. Antony, S. Ehrlich and H. Krieg, *The Journal of Chemical Physics*, 2010, **132**, 154104.
- 13 J. K. Nørskov, J. Rossmeisl, A. Logadottir, L. Lindqvist, J. R. Kitchin, T. Bligaard and H. Jónsson, *J. Phys. Chem. B*, 2004, **108**, 17886–17892.
- 14 Y. Zheng, Y. Jiao, Y. Zhu, L. H. Li, Y. Han, Y. Chen, A. Du, M. Jaroniec and S. Z. Qiao, *Nat Commun*, 2014, **5**, 3783.
- 15 J. K. Noerskov, T. Bligaard, A. Logadottir, J. R. Kitchin, J. G. Chen, S. Pandalov and U. Stimming, *ChemInform*, , DOI:10.1002/chin.200524023.
- 16 A. Kong, M. Peng, H. Gu, S. Zhao, Y. Lv, M. Liu, Y. Sun, S. Dai, Y. Fu, J. Zhang and W. Li, *Chemical Engineering Journal*, 2021, **426**, 131234.
- 17 Y. He, F. Yan, X. Zhang, C. Zhu, Y. Zhao, B. Geng, S. Chou, Y. Xie and Y. Chen, *Advanced Energy Materials*, **n/a**, 2204177.
- 18 M. Qu, Y. Jiang, M. Yang, S. Liu, Q. Guo, W. Shen, M. Li and R. He, *Applied Catalysis B: Environmental*, 2020, **263**, 118324.
- 19 X. Ma, H. Xiao, Y. Gao, M. Zhao, L. Zhang, J. Zhang, J. Jia and H. Wu, *J. Mater. Chem. A*, 2023, **11**, 3524–3534.
- 20 W. Li, B. Feng, L. Yi, J. Li and W. Hu, *ChemSusChem*, 2021, **14**, 730–737.
- 21 R. Jiang, Y. Da, J. Zhang, H. Wu, B. Fan, J. Li, J. Wang, Y. Deng, X. Han and W. Hu, *Applied Catalysis B: Environmental*, 2022, **316**, 121682.
- 22 Y. Pei, S. Guo, Q. Ju, Z. Li, P. Zhuang, R. Ma, Y. Hu, Y. Zhu, M. Yang, Y. Zhou, J. Shen and J. Wang, *ACS Appl. Mater. Interfaces*, 2020, **12**, 36177–36185.
- 23 W. Jiang, J. Wang, Y. Jiang, Y. Wu, B. Liu, X. Chu, C. Liu, G. Che and Y. Lu, *J. Mater. Chem. A*, 2023, **11**, 2769–2779.
- 24 Y. Zang, D.-Q. Lu, K. Wang, B. Li, P. Peng, Y.-Q. Lan and S.-Q. Zang, *Nat Commun*, 2023, **14**, 1792.

- 25 T. Xu, D. Jiao, M. Liu, L. Zhang, X. Fan, L. Zheng, W. Zheng and X. Cui, *Advanced Science*, 2023, **10**, 2205605.
- 26 X. Teng, J. Wang, L. Ji, W. Tang and Z. Chen, *ACS Sustainable Chem. Eng.*, 2018, **6**, 2069–2077.
- 27 K. T. Le, N. N. T. Pham, Y.-S. Liao, A. Ranjan, H.-Y. Lin, P.-H. Chen, H. Nguyen, M. Y. Lu, S. G. Lee and J. M. Wu, *J. Mater. Chem. A*, 2023, **11**, 3481–3492.
- 28 C. Liu, Q. Chen, Q. Hao, X. Zheng, S. Li, D. Jia, T. Gong, H. Liu and J. Zhang, *International Journal of Hydrogen Energy*, 2019, **44**, 4832–4838.
- 29 J. Shen, Q. Li, W. Zhang, Z. Cai, L. Cui, X. Liu and J. Liu, *J. Mater. Chem. A*, 2022, **10**, 5442–5451.
- 30 M. J. Jang, J. Yang, J. Jeong, G. H. Kim, C. Y. Kwon, N. V. Myung, K. H. Lee and S. M. Choi, *ACS Sustainable Chem. Eng.*, 2021, **9**, 12508–12513.
- 31 C. Liang, W. Cao, L. Zhou, P. Yang, X. Zhao, P. Zhao, R. Qiu, L. Yang, Q. Huang and D. Astruc, *ChemCatChem*, 2020, **12**, 1647–1652.
- 32 C. Yang, R. Zhao, H. Xiang, J. Wu, W. Zhong, W. Li, Q. Zhang, N. Yang and X. Li, *Advanced Energy Materials*, 2020, **10**, 2002260.
- 33 T. Cui, J. Chi, J. Zhu, X. Sun, J. Lai, Z. Li and L. Wang, *Applied Catalysis B: Environmental*, 2022, **319**, 121950.
- 34 P. Shen, B. Zhou, Z. Chen, W. Xiao, Y. Fu, J. Wan, Z. Wu and L. Wang, *Applied Catalysis B: Environmental*, 2023, **325**, 122305.
- 35 Y. Yu, S. J. Lee, J. Theerthagiri, Y. Lee and M. Y. Choi, *Applied Catalysis B: Environmental*, 2022, **316**, 121603.
- 36 Y. Jeong, S. Shankar Naik, Y. Yu, J. Theerthagiri, S. J. Lee, P. L. Show, H. C. Choi and M. Y. Choi, *Journal of Materials Science & Technology*, 2023, **143**, 20–29.
- 37 G. Liu, T. Nie, H. Wang, T. Shen, X. Sun, S. Bai, L. Zheng and Y.-F. Song, *ACS Catal.*, 2022, **12**, 10711–10717.
- 38 S. Ge, L. Zhang, J. Hou, S. Liu, Y. Qin, Q. Liu, X. Cai, Z. Sun, M. Yang, J. Luo and X. Liu, *ACS Appl. Energy Mater.*, 2022, **5**, 9487–9494.
- 39 J. Wang, X. Guan, H. Li, S. Zeng, R. Li, Q. Yao, H. Chen, Y. Zheng and K. Qu, *Nano Energy*, 2022, **100**, 107467.
- 40 K. Deng, Q. Mao, W. Wang, P. Wang, Z. Wang, Y. Xu, X. Li, H. Wang and L. Wang, *Applied Catalysis B: Environmental*, 2022, **310**, 121338.
- 41 D. Qi, S. Liu, H. Chen, S. Lai, Y. Qin, Y. Qiu, S. Dai, S. Zhang, J. Luo and X. Liu, *Mater. Chem. Front.*, 2021, **5**, 3125–3131.
- 42 M. Zhang, Z. Wang, Z. Duan, S. Wang, Y. Xu, X. Li, L. Wang and H. Wang, *J. Mater. Chem. A*, 2021, **9**, 18323–18328.
- 43 S. Chen, C. Wang, S. Liu, M. Huang, J. Lu, P. Xu, H. Tong, L. Hu and Q. Chen, *J. Phys. Chem. Lett.*, 2021, **12**, 4849–4856.
- 44 Z. Feng, T. Shi, W. Liu, W. Zhang and H. Zhang, *International Journal of Energy Research*, 2022, **46**, 15938–15947.

- 45 J. Hou, X. Peng, J. Sun, S. Zhang, Q. Liu, X. Wang, J. Luo and X. Liu, *Inorg. Chem. Front.*, 2022, **9**, 3047–3058.
- 46 S. Zhang, C. Zhang, X. Zheng, G. Su, H. Wang and M. Huang, *Applied Catalysis B: Environmental*, 2023, **324**, 122207.
- 47 W. Fang, J. Dang, Y. Hu, Y. Wu, S. Xin, B. Chen, H. Zhao and Z. Li, *Electrochimica Acta*, 2023, **439**, 141682.
- 48 X. Liu, H. Mao, G. Liu, Q. Yu, S. Wu, B. Li, G. Zhou, Z. Li and L. Wang, *Chemical Engineering Journal*, 2023, **451**, 138699.
- 49 Q. Yu, X. Liu, G. Liu, X. Wang, Z. Li, B. Li, Z. Wu and L. Wang, *Advanced Functional Materials*, 2022, **32**, 2205767.
- 50 Y. Guo, X. Liu, Y. Zang, Y. Wu, Q. Zhang, Z. Wang, Y. Liu, Z. Zheng, H. Cheng, B. Huang, Y. Dai and P. Wang, *J. Mater. Chem. A*, 2022, **10**, 17297–17306.
- 51 A. Zhang, H. Liu and C. Wang, *Electrochimica Acta*, 2022, **435**, 141406.